RSC Advances

ROYAL SOCIETY OF CHEMISTRY

www.rsc.org/advances

Nano Ag_5 cluster tip probing the vertical transfer of $CO_{(ads)}$ adsorbed on Ag(110) with simulated inelastic electron tunneling spectroscopy

Shao-Yu Lu and Jyh-Shing Lin*

Department of Chemistry, Tamkang University

Tamsui, Taiwan 25137

Abstract:

Nano Ag_5 cluster tip probing the vertical transfer of $CO_{(ads)}$ adsorbed on the Ag(110) surface has been investigated with simulated inelastic electron tunneling spectroscopy (IETS) generated by combining DFT-based molecular dynamic simulations with a Fourier transform of auto-correlation function of the derivative of local density of states (FT-ACF-δLDOS). It is found that tunneling conductance generated based on the trajectories of LDOS is significantly increased as a nano Ag_5 cluster tip is introduced and their vibrational amplitudes of low-frequency modes are enhanced in IETS. In addition, the IETS shows the doublet feature in the regions of low-frequency mode, i.e. frustrated-rotation, and high-frequency mode, i.e. C-O stretching, respectively, due to the change of geometry of $CO_{(ads)}$ leading to the transfer of $CO_{(ads)}$ adsorbed on the Ag(110) surface to a nano Ag_5 cluster tip. Furthermore, an anharmonic coupling between frustrated-rotation and C-O stretching mode is investigated by using a time-resolved IETS analysis. Finally, the key issue regarding to the activation of low-frequency modes by a nano Ag_5 cluster tip to cause the transfer of $CO_{(ads)}$ adsorbed on Ag(110) surface is addressed.

Introduction:

For more than two decades, scanning tunneling microscopy (STM) tip [1-2] have been used to position molecules on metal surfaces and to probe their electronic properties with atomic scale. In addition, the tunneling electrons from an STM tip can be used as a non-thermal energy source to induce electronic vibrational excitation of adsorbates that cause various controllable surface chemical reactions, such as vertical manipulation,[3-4] rotation,[5-6] dehydrogenation,[7-8] or lateral hopping process.[9-10] The corresponding inelastic electron tunneling spectroscopy (IETS)[11] can measure the change in tunneling conductance as electrons excite vibrations and is a powerful technique for the identification of vibrational signatures of single chemisorbed species on metal surfaces to predict and understand both bond-weakening and bond-breaking processes. In 2001, Ho et al.[12] successfully demonstrated a tip-induced vertical transfer of $CO_{(ads)}$ adsorbed on the Ag(110) surface by combining both STM topological image and IETS measurement, that is, the $CO_{(ads)}$ is vertically transferred from the Ag(110) surface to the tip by dosing the electrons into molecule. In 2002, Persson[13] followed the same strategy to investigate the lateral hopping process for $CO_{(ads)}$ adsorbed on the Pd(110) surface and it was found that its hopping rate is strongly related to intramolecular high-frequency stretching mode in IETS. Additionally, they believed that both vertical and lateral translations for the $CO_{(ads)}$ adsorbed on surface are induced by an anharmonic coupling between low-frequency modes (frustrated-translation and frustrated-rotation) and high-frequency vibrational mode (approximately 240 meV, C-O stretching mode).

Over past few years, theoretical research works have been devoted to developing the new methodology to simulate STM images and vibrational inelastic electron tunneling for providing more insights into the nature of the electron-vibration coupling in tunneling-current-induced reaction process[14-18]. Luo and co-workers [19] successfully generated IETS for $CO_{(ads)}$ adsorbed on Cu(100) based on Tersoff-Hamann (TH) approximation, [20-21] in which the tunneling conductance

is only proportional to local density of states (LDOS) at near Fermi level. In addition, G. Kirzenow's research group have generated the simulated IETS for identifying vibrational signatures of the propanedithiolate (PDT) molecule in Gold-thiol molecular junction and provide a good comparison with the experiment IETS results[22-24]. More recently, an approach beyond TH approximation, which includes electron-phonon coupling effect, has been successful to calculate the IETS for atomic-gold wires, molecular junction and single molecule adsorbed on metal surfaces by using nonequilibrium Green's functions (NEGF)[25-28]. In addition, Flipse and co-workers simulated $CO_{(ads)}$ on Cu(100) including tip effect to demonstrate how chemically functionalized STM tips modify the IETS intensity with respect to their vibrational modes[29-30]. Although these simulated IETS successfully provide a better understanding of electron tunneling process for $CO_{(ads)}$ adsorbed on the Cu(100) surface, the detailed reaction mechanism of tunneling-current-induced vertical transfer of $CO_{(ads)}$ adsorbed on the Ag(110) surface is still lacking due to the fact that these calculated IETS are generated based on static approach with harmonic approximation. Consequently, the effects of both temperature and tip on adsorption dynamics should be taken into account in the calculation to realize an anharmonic coupling for the adsorbate-surface system. Therefore, in this theoretical study, we will present a novel computational scheme to simulate IETS of $CO_{(ads)}$ adsorbed on the Ag(110) surface at finite temperature by using DFT-based molecular dynamic simulations in combination with a Fourier transform of auto-correlation function of the derivative of local density of states (FT-ACF-δLDOS). Furthermore, a nano Ag_5 cluster tip is introduced to accurately describe the interaction between a tip and the sample. In addition, the effect of a tip on adsorption dynamics of $CO_{(ads)}$ adsorbed on the Ag(110) surface is investigated to understand the correlation between the orientation of $CO_{(ads)}$ molecule axis and its tunneling conductance during dynamic simulation at finite temperature. Finally, we will explore the corresponding anharmonic coupling between low-frequency and high-frequency modes of $CO_{(ads)}$ by using a short-time Fourier transform (STFT) approach to provide an insight into the reaction dynamics for the vertical transfer of $CO_{(ads)}$ adsorbed on the Ag(110) surface.

The ground state properties for $CO_{(ads)}$-Ag(110) and $Ag_{5(tip)}$-$CO_{(ads)}$-Ag(110)

To calculate both electronic properties and STM images, we employed the fully *ab-initio* density functional theory (DFT) code *SIESTA* [31]. The exchange-correlation energy has been considered within the van-der Waal's density functional (vdW-DF)[32] to take into account the weak interaction between the CO and Ag(110) surface. The double zeta polarized (DZP) basis set is chosen for all atoms (Ag, C, and O). The localization radii of basis functions are determined from an energy cutoff of 0.01 Ry. The Kohn-Sham orbitals are expanded in a localized basis with a mesh cutoff of 150 Ry. For all adsorbed systems, a periodic 4-atom-layer slab with 15 Å of vacuum and a 2 x 2 x 1 Monkhorst-Pack k-point mesh are used [33]. Our calculations of tunneling conductance to generate the STM images are based on the Bardeen approximation as following:

$$\frac{dI}{dV}(x,y,V) = \frac{2\pi e}{\hbar}\sum_s [f(\varepsilon_t) - f(\varepsilon_s)]|M_{ts}|^2\delta(\varepsilon_t - \varepsilon_s + eV) \quad (1)$$

Here $f(\varepsilon)$ is the Fermi-Dirac function, the energies ε_t and ε_s are referred to the Fermi levels of a tip and sample, respectively, and V is the applied bias voltage. The Bardeen's tunneling matrix element (M_{ts}), which couples between sample wavefunction (ψ_s) and tip wavefunction (ψ_t) can be represented by a flux through a separation surface (S) as following:

$$M_{ts} = \frac{h}{2m}\int_s (\psi_s \nabla\psi_t^* - \psi_t^* \nabla\psi_s) dS \quad (2)$$

A simple model to evaluate the Bardeen's tunneling matrix is based on the TH approximation in which the wavefunction of a tip (ψ_t) is approximated as a symmetric s-wave orbital. To include the effect of a tip on adsorption dynamics of adsorbed systems during tunneling-current-induced process, we introduce a nano Ag_5 cluster tip in connection with remaining original sample

wavefunction (ψ_s) in our calculations. As a result the Bardeen's tunneling matrix can be derived to be only proportional to LDOS of sample at near Fermi energy as following:

$$|M_{ts}|^2 \propto \sum|\Psi_s(x,y,z)|^2\delta(E-E_F) = LDOS(x,y,z,E_F) \quad (3)$$

As temperature is lowered under room temperature, the Fermi-Dirac distribution can be approximated as a step function. Therefore, the equation (1) used to generate the tunneling conductance can be simply rewritten as following:

$$\frac{dI}{dV}(x,y,V)_{z=r_0} \propto LDOS(x,y,z,E_F) = \int_{E_F}^{E_F+\delta\varepsilon} LDOS_{3D_{grid}}(x,y,z,E)dE_{z=r_0} \quad (4)$$

Consequently, the tunneling conductance at a specific position (x,y) can be generated to produce the STM contour maps in a constant-height mode (the height of STM-tip: r_0) by integrating the LDOS in 3-dimension spatial grids over a small energy range ($\delta\varepsilon$) at Fermi level (E_F). The final form of the total tunneling conductance from a tip into the sample can be derived from the equation (4) to represent approximately as the LDOS in an x-y plane (N_x and N_y are the total number of grids in the a and b lattice direction).

$$\frac{dI}{dV}(V) \propto LDOS(r_0,E_F) = \int_0^{N_x}\int_0^{N_y}\int_{E_F}^{E_F+\delta\varepsilon} LDOS_{3D_{grid}}(x,y,z,E)dxdydE_{z=r_0} \quad (5)$$

In this study we introduce two kinds of nano Ag_5 cluster tips, which is a compressed trigonal-bipyramid tip ($Ag_{5(trigonal\text{-}tip)}$) and a w-shaped planar tip ($Ag_{5(planar\text{-}tip)}$), respectively (as suggested by previous theoretical studies[34-35]) to investigate the effect of a tip on the adsorption geometries and their tunneling currents for $CO_{(ads)}$ adsorbed on Ag(110) surface. A nano Ag_5 cluster tip is placed above the $CO_{(ads)}$-Ag(110) (the tip-O distance is approximately 3.0 Å). The optimized structures for each adsorbed systems and their corresponding STM images are shown in Figure 1.

Based on the calculated results the average distance between the $CO_{(ads)}$ and Ag(110) become slightly longer (from 2.311 Å to 2.361 Å) as a nano Ag_5 cluster tip is introduced and different electronic structure can be observed on the basis of the local density distribution around the Fermi energy, resulting in different STM topographic images. The experimental STM imaging map is also shown in Figure 1(e) for comparison. To realize the structural effect of the tip on their STM images, we further examine how the frontier molecular electronic states couple to the metallic electronic states with and without the effect of a tip. By analyzing the projected density of states (PDOS) for the $CO_{(ads)}$ molecule and their neighboring Ag surface atom and nano Ag_5 cluster tip atoms as shown in Figure 2, there is a higher intensity of a nano Ag_5 cluster tip state around the Fermi energy for the $Ag_{5(planar\text{-}tip)}$-$CO_{(ads)}$-Ag(110). It is proposed that there is a significantly orbital overlap between a nano Ag_5 cluster tip and the surface leading to their strong coupling when the tunneling process occurs. Obviously, the calculated STM image for $Ag_{5(planar\text{-}tip)}$-$CO_{(ads)}$-Ag(110) can be divided into two groups, the larger bright spot corresponding to the contribution of a nano Ag_5 cluster tip state and the central small bright spot as shown in Figure 1(d) corresponding to that of $CO_{(ads)}$ which are in a good agreement with the experimental STM results.

Temperature effects on adsorption dynamics for both $CO_{(ads)}$-Ag(110) and $Ag_{5(tip)}$-$CO_{(ads)}$-Ag(110)

To further investigate the thermal effect as the electron tunneling from a tip into the adsorbed system, we employed the density functional theory-based molecular dynamic (DFT-based MD) simulation, to calculate the $CO_{(ads)}$ adsorbed on the Ag(110) surface with and without a nano Ag_5 cluster tip at finite temperature. The DFT-based MD simulations are performed by using the same program SIESTA. All of the model systems are calculated at constant temperature (NVT) using Nosé–Hoover thermostat [36-37] for 7.0 ps with a time step of 0.5 fs at 50 K. Based on the experimental conditions, the STM is located above the substrate around the 3.0Å. Therefore, the distance between the bottom most Ag atom and O atom of CO adsorbed molecule is set to 3.0Å. After the geometries are optimized, the local minimum structures are used as the initial structural

models to run the MD simulation as shown in Figure 1. During the MD simulation, only the bottom 2 layers of Ag slab and top most Ag atom of a nano Ag5 cluster tip are constrained. The first part of DFT-based MD simulation is to reach an equilibration phase for at least 1.0ps. Then, the second part of the simulation, which lasts for 6 ps, is followed by collecting data over the temperature-controlled dynamic trajectories to generate a time-dependent autocorrelation function of the derivative of local density of states ($\mathrm{ACF} - \delta LDOS(r_0, E_F)$).

The temperature-controlled dynamic trajectories of $CO_{(ads)}$ during 6ps simulations for each adsorbed-surface systems are examined in Figure 3(a). First, the adsorbed $CO_{(ads)}$ was found to be stably located on the top site without a tip. Then, as a nano $Ag_{5(trigonal\text{-}tip)}$ cluster tip is introduced, the $CO_{(ads)}$ is slightly diffuse above the top site and the flipping rate for $CO_{(ads)}$ is significantly increased. It suggested that the interaction between the $CO_{(ads)}$ and surface is weakening. Finally, when a nano $Ag_{5(planar\text{-}tip)}$ cluster tip is introduced, the $CO_{(ads)}$ firstly adsorbed on the top site and then a 180^o rotation of $CO_{(ads)}$ occurs at approximately 3ps to move from the surface to a nano $Ag_{5(planer\text{-}tip)}$ cluster tip. To further investigate the electronic properties during the reaction, we collected the trajectories of LDOS at the tip position for the adsorbed systems with and without a tip for each MD simulations. As shown in Figure 3(b) the tunneling conductance is strongly dependent on the effect of a nano Ag_5 cluster tip. The average tunneling conductance of $Ag_{5(planar\text{-}tip)}$-$CO_{(ads)}$-Ag(110) is found to be more conductive, which is 1.74 and 13.97 times of $Ag_{5(trigonal\text{-}tip)}$-$CO_{(ads)}$-Ag(110) and $CO_{(ads)}$-Ag(110), respectively. This tip-enhanced tunneling conductance might increase the coupling between the surface and adsorbate leading to a higher possibility for the transfer process.

Simulated IETS for $CO_{(ads)}$-Ag(110) and $Ag_{5(tip)}$-$CO_{(ads)}$-Ag(110)

According to Fermi Golden's rule [38], the adsorption line shape of underlying perturbation is generated by considering light-matter cross section interaction and it can be calculated as a Fourier

transform of the autocorrelation function by using molecular dynamic simulation. For example, the Infrared adsorption spectrum $I^{IR}(\omega)$ and Raman spectrum $I^{Raman}(\omega)$ can be simulated by a Fourier transform of the dipole moment (μ) autocorrelation function $\langle\mu(t)\mu(0)\rangle$ and polarizability (α) autocorrelation function $\langle\alpha(t)\alpha(0)\rangle$, respectively (as discussed by our previous theoretical studies [39-42]). Following the same strategy, by considering that (1) the IETS is related to the second derivatives of I (tunneling current) with respect to V and (2) the IETS intensity is proportional to the change in LDOS at specific molecular vibration, Qi, $(\frac{\partial LDOS(r_0,E_F)}{\partial Qi})^2$, the IETS can be generated by using a Fourier transform of the autocorrelation of the derivative of LDOS ($\delta LDOS$) as following:

$$I^{IETS}(\omega) \propto \int_{-\infty}^{\infty}\langle\delta LDOS(r_0,E_F,t)\delta LDOS(r_0,E_F,0)\rangle\, e^{i\omega t}dt \qquad (6)$$

The calculated IETS for $CO_{(ads)}$ adsorbed on the Ag(110) surface for each adsorbed systems are shown in Figure 4(a). Table 1 lists all the calculated vibrational modes and corresponding experimental IETS results. In the low-frequency region, the IETS active peak at 48 cm^{-1} (6 meV) can be assigned to the frustrated translation, the active peak at 144 cm^{-1} and 166 cm^{-1} (17 meV and 20 meV) can be assigned to doublet frustrated rotation and the active peak at 266 cm^{-1} (33 meV) is the Ag-C stretching. In the high-frequency region, the IETS active peak at 1991 cm^{-1} and 2033 cm^{-1} (246 meV and 252 meV) can be assigned to the C-O stretching. Due to all IETS active vibrational modes are under the low-energy region (< 0.5eV), the Bardeen formalism are still valid. Indeed, the active peaks on IETS by using MD are in a good agreement with the experimental results and even much closer to the experimental results than that of normal mode calculations as shown in Table 1. Furthermore, it is found that the tunneling amplitude of the IETS peaks in low-frequency region is strongly dependent on the influence of a tip. Then, these tip-induced motions in low-frequency region will cause structural changes of $CO_{(ads)}$ adsorbed on the surface. As a result, the lateral hopping and vertical transfer of $CO_{(ads)}$ adsorbed on the Ag(110) surface can

be investigated by monitoring the atomic trajectories through molecular dynamics simulations.

Anharmonic coupling for $Ag_{5(planar\text{-}tip)}$-$CO_{(ads)}$-Ag(110) by STFT analysis

To further investigate the doublet features which appear in both of the frustrated rotation and C-O stretching, we implement previous Fourier transform of the autocorrelation function of the derivative of LDOS ($\delta LDOS$) by introducing the short-time Fourier transform (STFT)[41] approach to generate the time-resolved IETS as the following equation:

$$I^{IETS}(\tau,\omega) \propto \int_{-\infty}^{\infty} \langle \delta LDOS(r_0, E_F, t)\delta LDOS(r_0, E_F, 0)\rangle\, h(t+\tau)e^{i\omega t}dt \quad (7)$$

$$\mathrm{h}(\mathrm{t}+\tau) = \begin{cases} 1, & \tau \le t \le T+\tau \\ 0, & otherwise \end{cases}$$

where $\mathrm{h}(\mathrm{t}+\tau)$ is the rectangular window function, τ is the delay time, $I^{IETS}(\tau,\omega)$ is a time-resolved power spectrum, which is called a spectrogram of IETS, and T is the window length whose size determines the resolution of frequency of a time-resolved power spectrum. In this study, 2.0 ps of a window length (T) is adopted. As shown in Figure 5, the spectrogram can provide both of time and frequency domains to explore the evolution of all vibrational modes in IETS for $Ag_{5(planar\text{-}tip)}$-$CO_{(ads)}$-Ag(110) along the vertical transfer reaction pathway to investigate the correlation between the low-frequency mode and high-frequency modes.

Based on the structural evolution of $CO_{(ads)}$ adsorbed on Ag(110) surface and corresponding IETS spectrogram the whole vertical transfer process can be divided into three stages. Firstly, before the $CO_{(ads)}$ is transferred to the tip, the frustrated rotation and the C-O stretching are assigned at 166 cm^{-1} (20 meV) and 1991 cm^{-1} (246 meV), respectively. Secondly, as the vertical

transfer proceeds at nearly 3ps, the nano Ag_5 cluster tip will induce Ag-C bond weakening leading to a red-shifted of the frustrated rotation (from 166 cm^{-1} to 144 cm^{-1}) and it also accompanies with a blue-shifted of C-O stretching (from 1991 cm^{-1} to 2033 cm^{-1}). Thirdly, as the CO transfers from the surface to a nano Ag_5 cluster tip, the frustrated rotation and C-O stretching are returned to 166 cm^{-1} (20 meV) and 1991 cm^{-1} (246 meV), respectively. In contrast to the frustrated rotation, the frustrated translation still remains unchanged (6 meV) along the vertical transfer of $CO_{(ads)}$ on Ag(110) surface. These correlations between low-frequencies (frustrated rotation / frustrated translation) and high-frequency (C-O stretching) imply that there is higher anharmonic coupling for the (frustrated rotation v.s. C-O stretching) than that of (frustrated translation v.s. C-O stretching). Finally, by using single-frequency pass filter (SPFP)[42] analysis scheme, an anharmonic coupling arisen from the frustrated rotation can be further investigated. As shown in inserted figure of Figure 5, the tip-induced frustrated rotation at 166 cm^{-1} can be identified to the flipping motion of $CO_{(ads)}$ and it couples to the Ag-C stretching. On the other hand, the tip-induced frustrated rotation at 144 cm^{-1} can be identified to a rotation along the axis of surface normal and it shows a less dependence on the surface atom due to the weak interaction between the surface and $CO_{(ads)}$ when vertical transfer manipulation occurs.

Conclusion

By combing DFT-based MD simulations with a Fourier transform of autocorrelation function of the derivative of local density of states (FT-ACF-δLDOS), the IETS spectra for CO adsorbed on the Ag(110) surface have been successfully calculated and analyzed to investigate the effect of the nano Ag_5 cluster tip on adsorption dynamics and their tunneling conductance at finite temperature during the dynamics process. Our calculated results are summarized below. First, we found that the tunneling conductance generated based on the trajectories of LDOS is significantly increased as a nano Ag_5 cluster tip is introduced and their vibrational amplitudes of low-frequency modes (ex.

frustrated translation, frustrated rotation and Ag-C stretching) are enhanced in IETS spectrum. Second, the IETS spectrum shows the doublet feature at both low-frequency and high-frequency regions, that is, frustrated rotation and intramolecular C-O stretching, respectively, due to the change of geometry of $CO_{(ads)}$ adsorbed on the Ag(110) surface. Third, by combining the short-time Fourier transform (STFT) and single-frequency pass filter (SPFP) analysis schemes, an anharmonic coupling between the frustrated rotation and intramolecular C-O stretching has been confirmed. Finally, it is our hope that this study will stimulate further experimental efforts to provide more insights into the nature of electron-vibration coupling for investigating the STM-tip induced chemical reactions.

Acknowledgments

The authors would like to thank the National Council in Taiwan for financial support (grant nos. NSC 97-2113-M-032-003-MY3 and NSC 100-2113-M-032-002-) and the National Center for High Performance Computing and Tamkang University in Taiwan for the use of computational facilities.

References:

[1] G. Binnig, H. Rohrer, C. Gerber, E. Weibei, *Phys. Rev. Lett*. 49, 57, **(**1982**).**

[2] T. A. Jung, R. R. Schlittler, J. K. Gimzewski, *Nature*, 386, 696, (1997**).**

[3] H. J. Lee and W. Ho, *Science*, 286, 1719 (1999).

[4] J. I. Pascual, N. Lorente, Z. Song, H. Conrad and H.-P. Rust, *Nature*, 423, 525, (2003).

[5] L. J. Lauhon, W. Ho, *J. Phys. Chem. A*, 104, 2463, (2000).

[6] N. Henningsen, K. Franke, I. Torrente, G. Schulze, B. Priewisch, K. Ruck-Braun, J. Dokic, T. Klamroth, P. Saalfrank, J. Pascual. *J. Phys. Chem. C*, 111, 14843 (2007).

[7] T. Komeda, Y. Kim, Y. Fujita, Y. Sainoo, M. Kawai, *J. Chem. Phys*. 120, 5347, (2004).

[8] D. Riedel, M.-L. Bocquet, H. Lesnard, M. Lastapis, N. Lorente, P. Sonnet, G. Dujardin, *J. Am. Chem. Soc*. 131, 7344, (2009).

[9] J. A. Stroscio and R. J. Celotta, *Science*, 306, 242 (2004).

[10] M. Ohara, Y. Kim and M. Kawai, *Jap. J. Appl. Phys*. 45, 2022, (2006).

[11] B. C. Stipe, M. A. Rezaei ,and W. Ho, *Science*, 280, 1732, (1998).

[12] J. R. Hahn and W. Ho, *Phys. Rev. Lett*., 86, 166102, (2001).

[13] T. Komea, Y. Kim, M. Kawai, B. N. J. Persson, H. Ueba, *Science*, 295, 2055, (2002).

[14] N. Mingo and K. Makoshi, *Phys. Rev. Lett.*, 84, 3694, (2000).

[15] N. Lorente and M. Persson, *Faraday Discuss.*, 117, 277, (2000).

[16] N. Lorente and M. Persson, *Phys. Rev. Lett.*, 85, 2997, (2000).

[17] S. Tikhodeev, M. Natario, K. Makoshi, T. Mii and H. Ueba, *Surf. Sci,*. 463, 63, (2001).

[18] G. Teobaldi, M. Peñalba, A. Arnau, N. Lorente and W. A. Hofer, *Phys. Rev. B*, 76, 235407, (2007).

[19] H. Ren, J. Yang, Y. Luo, *J. Chem. Phys.*, 130, 134707, (2009).

[20] J. Tersoff, D. R. Hamann, *Phys. Rev. Lett.*, 50, 1998, (1983).

[21] J. Tersoff, D. R. Hamann, *Phys. Rev. B*, 31, 805, (1985).

[22] F. Demir, G. Kirczenow, *J. Chem. Phys*, 136, 014703 (2012).

[23] X. Li, J. He, J. Hihath, B. Xu, S. M. Lindsay, and N. J. Tao, *J. Am. Chem. Soc.* 128, 2135 (2006).

[24] J. Hihath, C. R. Arroyo, G. Rubio-Bollinger, N. Tao, and N. Agraït, *Nano Lett*. 8, 1673 (2008).

[25] J. Lykkebo, A. Gagliardi, A. Pecchia, and G. C. Solomon, *ACS Nano*, 7, 9183 (2013).

[26] M. Paulsson, T. Frederiksen, H. Ueba, N. Lorente, and M. Bradnbyge, *Phys. Rev. Lett.*, 100, 226604 (2008).

[27] A , Troisi, M. A. Ratner, *Nano Lett,* 6, 1784 (2006).

[28] G. C. Solomon, A. Gagliardi, A. Pecchia, T. Frauenheim, A. D. Carlo, J. R. Reimers, and N. S. Hush, *J. Chem. Phys.,* 124, 094704 (2006).

[29] M. Paulsson, T. Frederiksen, and M. Brandbyge, *Phys. Rev. B*, 72, 201101(R), (2005).

[30] E. T. R., Rossen, C. F. J. Flipse, and J. I. Cerdá, *Phys. Rev. B*, 87, 235412, (2013).

[31] J. M. Soler, E. Artacho, J. D. Gale, A. García, J. Junquera, P. Ordejón and D. Sánchez-Portal, *Journal of Phys. : Conden.Matt.*, 11, 2745, (2002).

[32] G. R-Perez, J. M. Soler, *Phys. Rev. Lett*., 103, 096102, (2009).

[33] H. J. Monkhorst, J. D. Pack, *Phys. Rev. B*, 13, 5188, (1976).

[34] J. Zhao, Y. Luo, G. Wang, Eur. *J. Phys. D,* 3, 309, (2001).

[35] B. K. Agrawal, S. Agrawal, P. Srivastava, S. Singh, *J. Nanopart. Res.* ,6 **,** 363, (2004).

[36] S. Nosé, *J. Chem. Phys*., 81, 511, (1984).

[37] W. G. Hoover, *Phys. Rev. A*, 31, 1695, (1985).

[38] D. A. McQuarrie, "*Statistical Mechanics*" (Harper and Row, New York, **1976**).

[39] J. S. Lin, S. Y. Lu, P. J. Tseng, W. C. Chou, *J. Comp. Chem*. 33, 1274, (2012).

[40] S. Y. Lu, J. S. Lin, *J. Chem. Phys*., 140, 024705, (2014).

[41] Y. T. Lee, J. S. Lin, *J. Comp. Chem*., 34, 2697, (2013).

[42] J. P. Su, Y. T. Lee, S. Y. Lu, J. S. Lin, *J. Comp. Chem*., 34, 32, 2806, (2013).

Figure Captions

Figure 1. (a) The optimized structure for $CO_{(ads)}$-Ag(110), $Ag_{5(trigonal\text{-}tip)}$-$CO_{(ads)}$ -Ag(110), and $Ag_{5(planar\text{-}tip)}$-$CO_{(ads)}$-Ag(110) and corresponding electronic structures of the LDOS at the Fermi energy. (b) The simulated STM image of $CO_{(ads)}$-Ag(110), (c)$Ag_{5(trigonal\text{-}tip)}$-$CO_{(ads)}$-Ag(110), (d) $Ag_{5(planar\text{-}tip)}$-$CO_{(ads)}$-Ag(110), (d) and the experimental STM result.

Figure 2. DOS projected onto the CO molecule (green line) and their neighboring Ag surface atom (blue line) and nano cluster Ag_5 tip atom (red line). From the top to bottom: the PDOS of $CO_{(ads)}$ adsorbed on Ag(110), $Ag_{5(trigonal\text{-}tip)}$-$CO_{(ads)}$ adsorbed on Ag(110) and $Ag_{5(planar\text{-}tip)}$-$CO_{(ads)}$ adsorbed on Ag(110)

Figure 3. (a) The dynamic trajectories of $CO_{(ads)}$ during 6ps DFTMD simulations and (b) corresponding LDOS(r_0,E_F) for each investigated systems, $CO_{(ads)}$ adsorbed on Ag(110) (red line), $Ag_{5(trigonal\text{-}tip)}$-$CO_{(ads)}$ adsorbed on Ag(110) (green line) and $Ag_{5(planar\text{-}tip)}$-$CO_{(ads)}$ adsorbed on Ag(110) (black line).

Figure 4. The calculated IETS spectrum for each investigated systems, $CO_{(ads)}$ adsorbed on Ag(110) (red line), $Ag_{5(trigonal\text{-}tip)}$-$CO_{(ads)}$ adsorbed on Ag(110) (green line) and $Ag_{5(planar\text{-}tip)}$-$CO_{(ads)}$ adsorbed on Ag(110) (black line) during 6ps DFTMD simulations.

Figure 5. The spectrogram obtained by STFT analysis for the IETS spectrum for the $Ag_{5(planar\text{-}tip)}$-$CO_{(ads)}$ adsorbed on the Ag(110) surface and corresponding structural changed during 6ps MD simulation. The two kinds of frustrated rotation motion are shown in inserted Figure by SFPF analysis.

Tables

Table 1. Calculated major IETS active peaks for $Ag_{5(trigonal\text{-}tip)}$-$CO_{(ads)}$ and $Ag_{5(planar\text{-}tip)}$-$CO_{(ads)}$ adsorbed on the Ag(111) surface at 50K. Normal mode calculation with different type of basis set (SZP, DZ, DZP) and experimental of IETS are also included for comparison.

Figure. 1

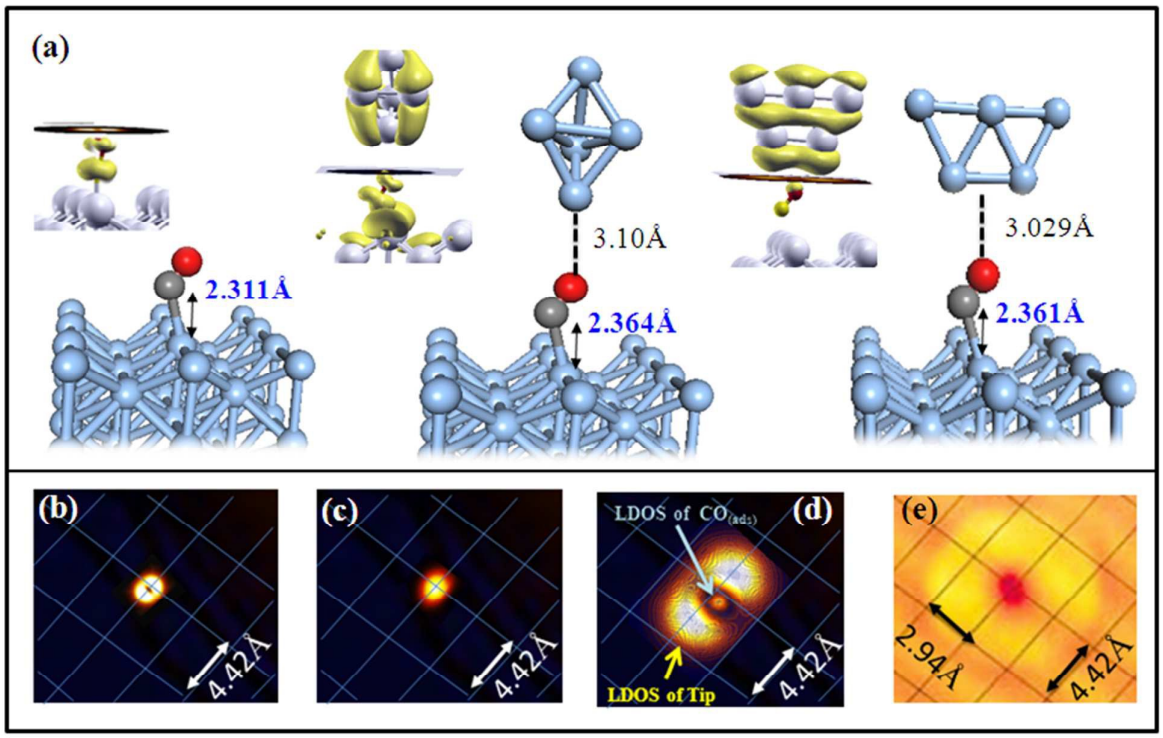

Figure 2.

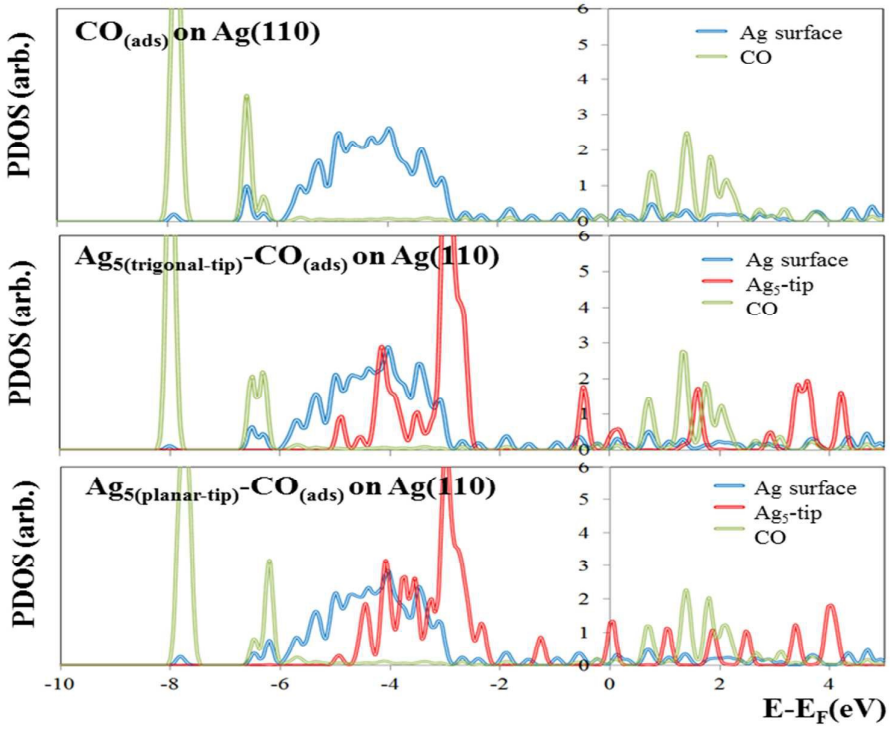

Figure 3.

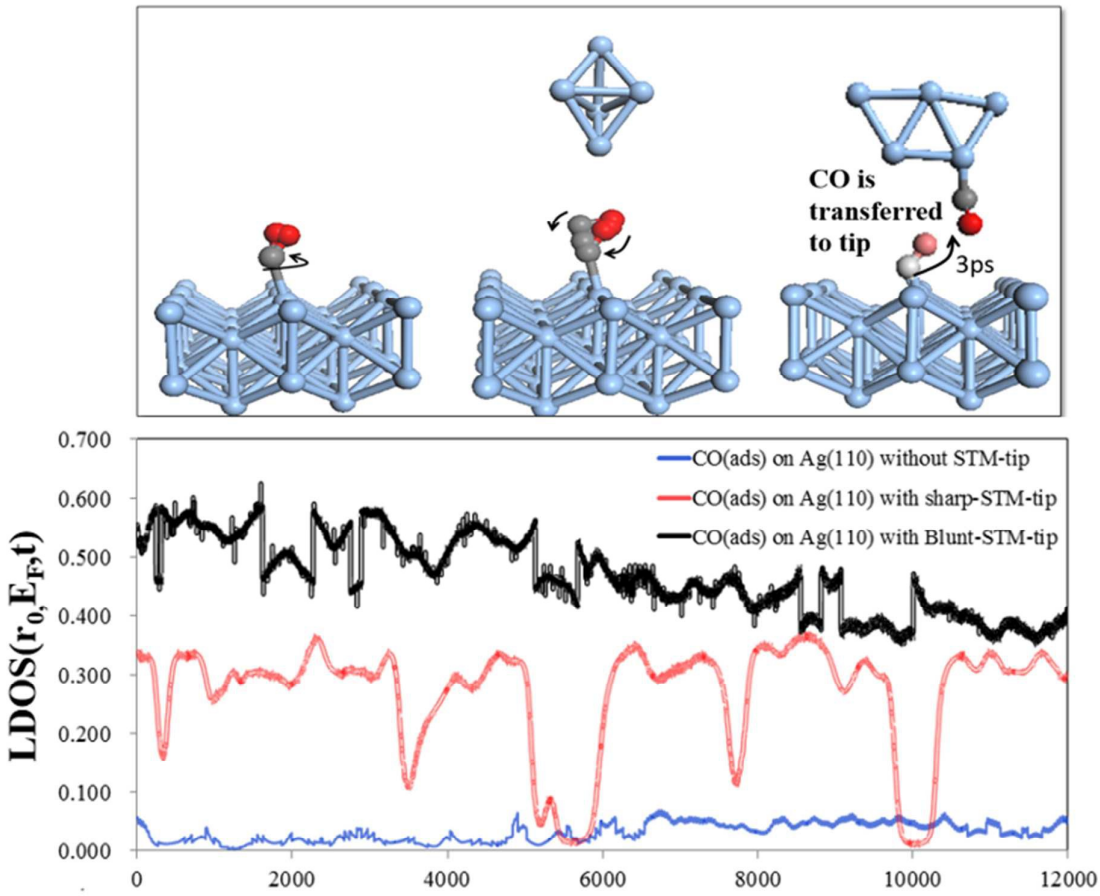

Figure 4.

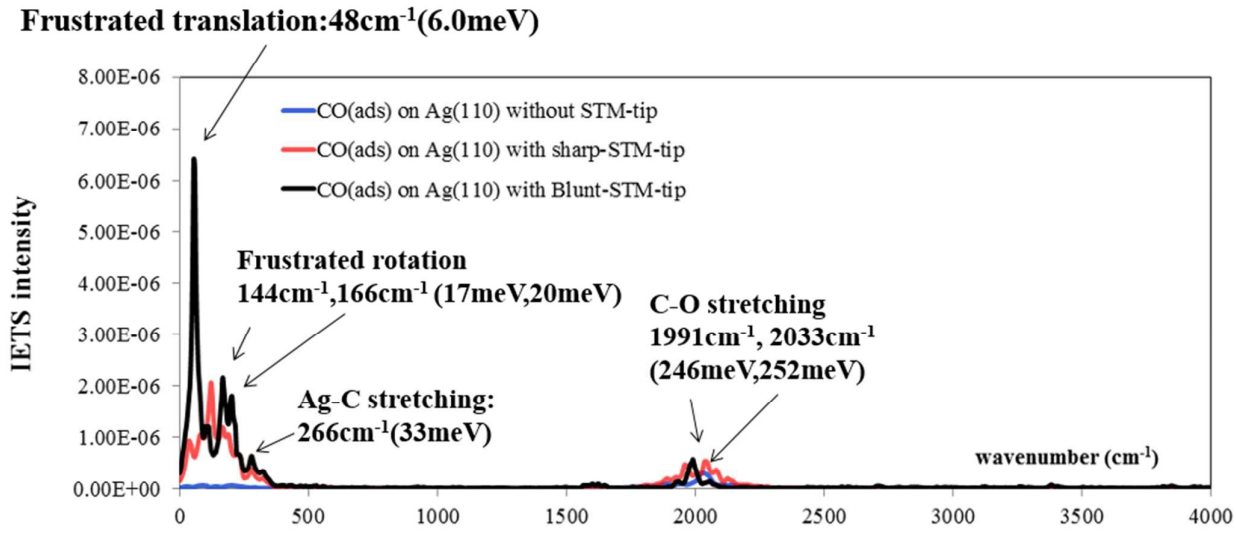

Figure 5.

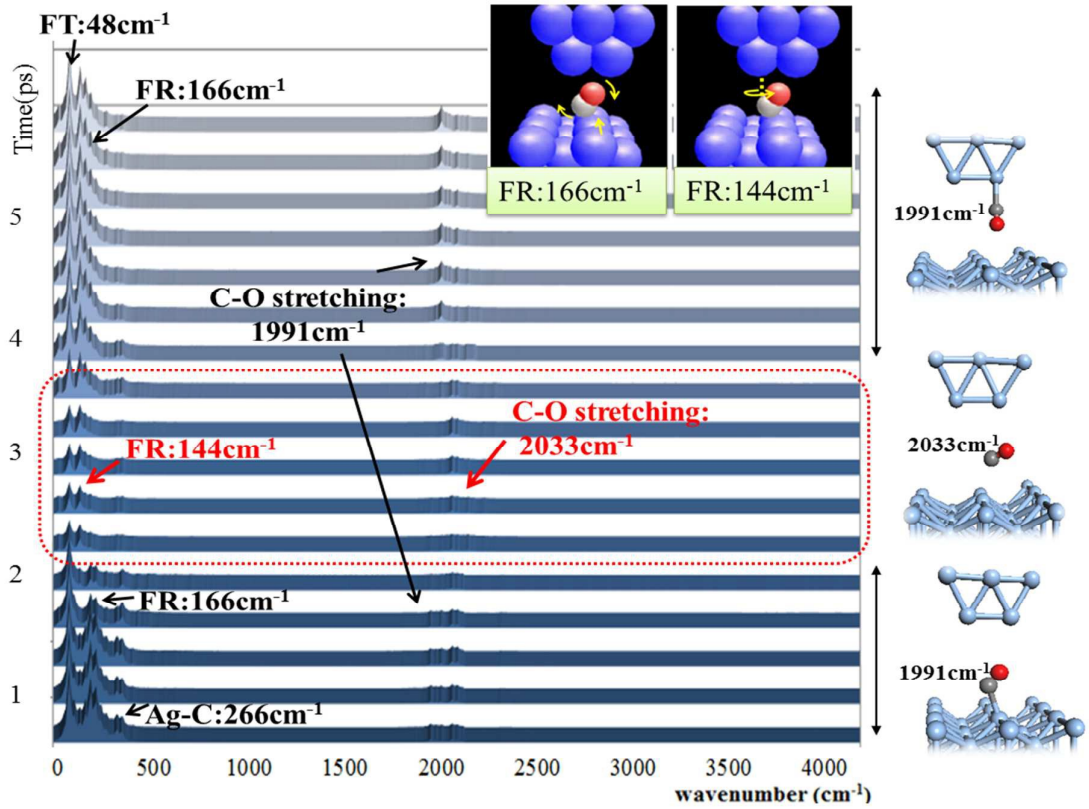

Table 1.

IETS spectrum	CO stretching (meV)	Ag-C stretching (meV)	Frustrated rotation(meV)	Frustrated translation(meV)
Experimental	263	33	18(20)	5
MD-Ag_5-(trigonal-tip) DZP	255(242)	34	16(20)	4
Static-Ag_5-(trigonal-tip) DZP	238	31	16	4
Static-Ag_5-(trigonal-tip) DZ	239	30	15	4
Static-Ag_5-(trigonal-tip) SZP	239	30	15	3
MD-Ag5-(planar-tip) DZP	252(247)	33	18(21)	6
Static-Ag5-(planar-tip) DZP	242	31	14	3
Static-Ag5-(planar-tip) DZ	242	30	13	3
Static-Ag5-(planar-tip) SZP	242	30	14	2